Gravitational Waves and the Laser Interferometer Space Antenna (LISA) and "Lab on a Chip"

by

Jessica Gifford

A PROJECT

submitted to

Oregon State University

University Honors College

in partial fulfillment of
the requirements for the
degree of

Honors Baccalaureate of Science in Physics (Honors Associate)

Presented 27 May 2011
Commencement June 2011

AN ABSTRACT OF THE THESIS OF

Jessica Gifford for the degree of Honors Baccalaureate of Science in Physics presented on May 27, 2011. Title: Gravitational Waves and the Laser Interferometer Space Antenna (LISA) .

Abstract approved: _____

Oksana Ostroverkhova

Improvements on the charge control measurements of the torsion pendulum, electron gun, and autocollimator system were conducted at the University of Washington in preparation for the fabrication of the final prototype of the Laser Interferometer Space Antenna (LISA) gravitational wave detector for NASA. One main cause of transient forces on LISA is solar charges in space that can cause unwanted torque on the test masses. Using a torsion pendulum as a geometric equivalent of the test masses, charge control measurements were conducted by producing a sinusoidal curve of the charge. The pendulum could be negatively or positively charged by an electron gun or a UV LED by increments as small as a pico-coulomb. The average charging for the UV LED is $3.5*10^{-14}$ C/s, and electron gun is $-4.4*10^{-14}$ C/s, which allows for very precise control.

Photocurrent of the UV LED and electron gun were measured by fabricating two new electron guns, one including an Einzel lens. Preliminary results showed that a current leakage powering the UV LED was a major source of error. To compensate for this error a battery system was built to power the UV LED separately from the electron gun. Subsequent results showed that, even with the battery improvement, no difference in current could be measured. To cut down on further current leakage a data acquisition program (DAQ) was designed to electronically control the power of the system. The results from varying the voltage using the

DAQ, showed that the photocurrent linearly increases and asymptotically approaches a maximum current. However, by moving the battery system, the current jumps drastically, which means that the production of photocurrent is yet to be conclusive.

Finally, the autocollimator was used to measure the torque on the pendulum with heterodyne interferometry. A system of thermometers was fabricated to measure the temperature inside and outside the autocollimating system. It was shown that the thermal noise fluctuation is 0.14^{o}C in the system. It is hypothesized that this fluctuation can be eliminated which will be enough to improve the sensitivity of the autocollimator by an order of magnitude.

Key Words: Torsion pendulum, Laser Interferometer Space Antenna (LISA), charge control, electron gun, UV LED, photocurrent, autocollimator, heterodyne interferometry, and the University of Washington.

Corresponding e-mail address: giffordj@onid.orst.edu

AN ABSTRACT OF THE THESIS OF

Jessica Gifford for the degree of Honors Baccalaureate of Science in Physics presented on May 27, 2011. Title: "Lab on a Chip" .

Abstract approved: _____

Oksana Ostroverkhova

Prototypes of a "Lab on a Chip" system that can make the sensors *in situ* in the device and then directly measure changes within a cell could greatly aid biologist in investigating changes within a variety of cells. At Oregon State University, an experimental setup was designed to trap and excite fluorescence of a particle or nano-sensor with and without a microfluidic device. An excitation laser at 532 nm and an optical trapping laser at 800 nm were used. The power of the excitation laser must be ~10 mW, which is low enough to cause minimal photo bleaching of the particles, and the power of the trapping laser must be ~5 mW for a 1 μm particle. One particle was trapped at a time by using confocal setting and aligning both lasers to hit the sample on the inverted microscope to within a few nano meters.

Proof of concept of the setup was then conducted using commercial Fluorospheres. The spectrum measured by this design matches the theoretical spectra provided by the particles' manufacturer demonstrating that the experimental design performs to specifications. Measurements were taken on the nano-sensors made by the collaborators at the chemistry department to verify that the setup is compatible with the new particles. First using only the excitation laser to excite and trap the sensors, different fluorescence peaks were measured for two samples of particles in pH ~2 and ~6 solutions. Because of photo bleaching, the behavior of

the spectra are indistinguishable from that of deprotonated peaks, however there was notable difference between the particles. The trapping laser was then reintroduced and verified that fluorescence measurements of a nano-sensor can be obtained with this experimental design.

Two other experiments were conducted, which confirm the proof of concept of this experimental design. Fluorescence data of K^+ ion sensitive sensors, which switch from deprotonated peaks, to protonated, using widefield excitation, was measured. This shows that the sensors behave as expected. Also, using this experimental technique developed, the setup was able to trap and measure the fluorescence of pH 2 and pH 7.5 sensors inside a microfluidic trap, and that the correct measurements can be taken with the setup even within a microfluidic trap.

Key Words: “Lab on a Chip”, *in situ*, Oregon State University, fluorescence, nano-sensors, photo bleaching, Fluorospheres, microfluidic, optical tweezers, deprotonated, protonated, and widefield.

Corresponding e-mail address: giffordj@onid.orst.edu

Gravitational Waves and the Laser Interferometer Space Antenna (LISA) and "Lab on a Chip"

by

Jessica Gifford

A PROJECT

submitted to

Oregon State University

University Honors College

in partial fulfillment of
the requirements for the
degree of

Honors Baccalaureate of Science in Physics (Honors Associate)

Presented 27 May 2011
Commencement June 2011

Honors Baccalaureate of Science in Physics project of Jessica Gifford presented on May 27, 2011.

APPROVED:

_____

Mentor, representing Physics: Oksana Ostroverkhova

_____

Committee Member, representing Physics: David McIntyre

_____

Committee Member, representing Physics: Henri Jansen

_____

Chair, Department of Physics: Henri Jansen

_____

Dean, University Honors College

I understand that my project will become part of the permanent collection of Oregon State University, University Honors College. My signature below authorizes release of my project to any reader upon request.

_____

Jessica Gifford, Author

Table of Contents

Chapter 1: Gravitational waves and the Laser Interferometer Space Antenna project

Table of Figures

Gravitational Waves and the Laser Interferometer Space Antenna (LISA)

1.1 Introduction

The Institute of Nuclear Technology at UW is one of many academic institutions and private companies contributing to the ESA-NASA joint project titled the *Laser Interferometer Space Antenna (LISA)* which will be the first gravitational wave detector in space, scheduled to launch in 2018 [1]. At the University of Washington, research is being done to develop methods for charge control and phase measurements of the satellites that make up LISA. The goals of this project are to demonstrate charge control of the satellites, improve these measurements by redesigning the electron gun that charges the system, and to reduce thermal noise inside the autocollimator detection system.

Ever since 1915 with the emergence of Einstein's Theory of General Relativity, the detection of gravitational waves has become one of the most challenging areas of experimental physics. General Relativity addresses the concern that there is no difference between a homogeneous gravitational field and an accelerated reference frame. This phenomenon is best explained with the famous Einstein elevator. First, a man on earth, in a non-accelerating elevator, drops a ball. His friend is in an elevator in space, with no gravitational field, which is accelerating upward such that, when he drops an identical ball, it appears to drop exactly the same as the other man on earth in his non accelerating reference frame. This comparison is shown in figure 1.1.1. This is known as the equivalence principle where, in one case, gravity is causing the ball to drop to the ground, and in the other case an accelerating reference frame causes the same motion. By introducing the notion of space-time curvature, which influences

the motion of objects by a homogeneous gravitational field, Einstein predicted that the equivalence principle does not hold, but that in fact the two can be distinguished from one another.

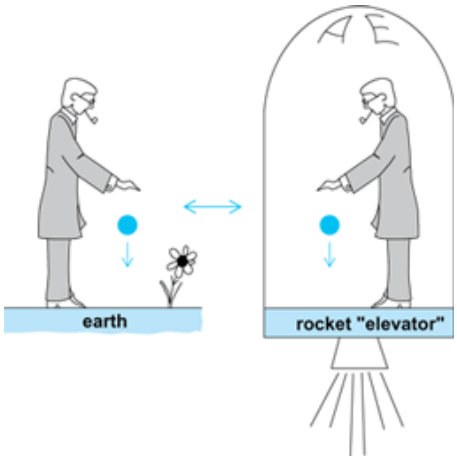

Figure 1.1.1: Einstein's elevator. To the left a man drops a ball on earth, and to the right a man drops a ball in an accelerating elevator in space with no gravity. Both men see the same motion of the ball dropping and cannot distinguish a difference from the homogenous gravitational field and the accelerating reference frame [2].

Einstein predicted that moving masses can produce propagating gravitational vibrations, or waves, that travel through space-time at the speed of light [1]. These vibrations are analogous to the vibrations of electromagnetic radiation that are produced by accelerating electric charges. Because gravity is a propagating wave, it can be represented as a coupled polarization of + and – that correspond to the stretching or squeezing of space-time caused by these waves. This causes the distances between two masses to oscillate by squeezing and stretching space-time. The amplitude of this wave is characterized by a dimensionless strain *h*, which is the fractional amount of stretching and squeezing [1]. Due to the perturbations in space time being very small, this strain is predicted to be on the order of 10^{-21}. A strain of 10^{-21} corresponds to measuring a change in distance between masses to be on the order of 10^{-18} m

for distances over km scale baselines [1].

LISA is located in space, which presents a significant advantage over other ground based detectors such as LIGO, which must overcome transient forces and noise, such as gravity, which are not present in space. Figure 1.1.2 is the design of LISA. LISA is set to follow the earth's orbit around the sun at an angular distance of approximately 20^{o}, or 50 million km. LISA will be composed of three satellites, each housing two cubical proof masses made of 46 mm gold-platinum alloy and coated in gold.

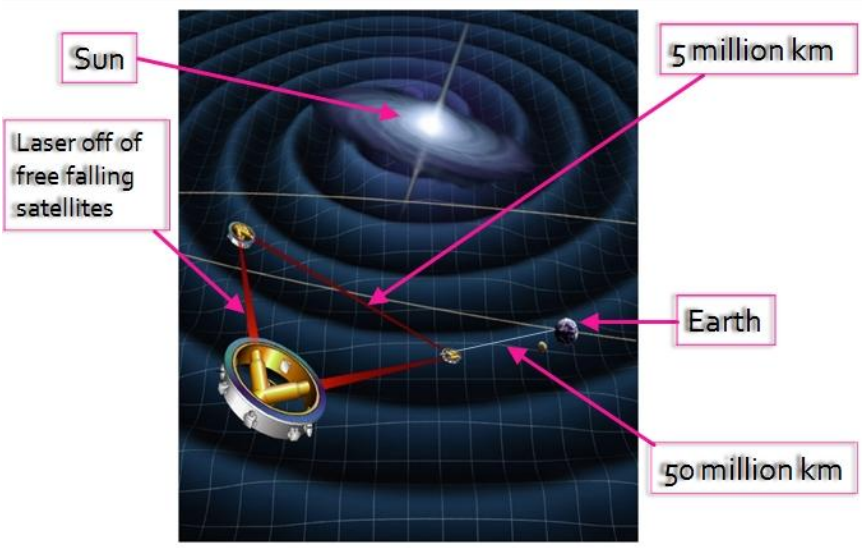

Figure 1.1.2: LISA Schematic shows the layout of LISA which follows earth's orbit by 50 million km. There are three satellites house proof masses that are 5 million km apart, and a laser is used to reflect light off the test masses. The time it takes to travel from proof mass to proof mass is measured, and any variations in time may correspond to perturbations of space-time by gravitational waves in space from a large mass.

Because LISA is in space, it needs to be shielded from solar winds, and charges. Each proof mass is in free fall to attain gravitational balance with no contact to any other component of the individual satellites including the housing. Each satellite is also not in contact with any

other satellite; only a laser beam goes between them. However, solar charges are predicted to leak into the system. Since the system will only attain a finite efficiency, the University of Washington has designed a charge control device to cancel out any excess charges that could cause non gravitational torque on the masses. Each satellite will be separated by 5 million km, which is approximately a million times greater than the arm lengths of earth based detectors. The distance allows for six times the sensitivity to the gravitational strain from that of grounded detectors, and ability to detect gravitational waves from farther objects in space [1]. LISA uses an interferometer to measure the change in distance of the masses due to gravitational waves. Because the speed of light is constant, any changes in time for the light to get from one test mass to the other will correspond to space-time being perturbed by the gravitational waves from a large mass source.

The gravitational group at the University of Washington has designed a geometric equivalent pendulum, as discussed below, to demonstrate charge control on the proof masses, and uses an autocollimator to measure the changes in distance between the masses.

1.2 Theory

All of the following theory discusses the various components specific to UW's and this thesis project rather than LISA as the overall NASA project. Because free fall cannot be precisely created on earth, the University of Washington uses a torsion pendulum to model the proof masses of LISA. This pendulum is housed in a pressurized chamber, at $3.0*10^{-9}$ Pa, while being suspended by a thin quartz fiber, and is not connected to any other charging or measuring components. With this design, the pendulum can simulate free fall to a finite precision attainable on the earth, and is therefore considered a geometric equivalent to the proof masses

of LISA. Torsion pendulums have been used in gravitational physics since 1853, and since then, over 100 designs have been published. However, they all follow the same basic design, shown in figure 1.2.1. A mass, in the case of figure 1.2.1 made of pyrex and tungsten, is suspended by a thin fiber and balanced in the horizontal plane. The fiber allows the mass to hang along the vertical gravitational field and therefore the forces of gravity and centrifugal acceleration of the earth are constant and homogenous in the vertical field, causing a quasi free fall, or floating in the horizontal plane [3].

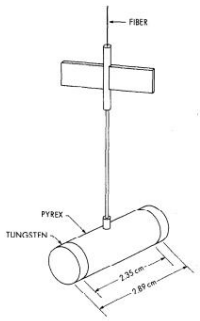

Figure 1.2.1: Simplified design of a basic torsion pendulum. A mass is suspended by a thin fiber and is balanced perfectly, such that the mass hangs along the vertical gravitational field. This allows weak forces, which cause horizontal torque of the pendulum, to be measured in the presence of large forces such as gravity in the vertical direction [3].

Torsion pendulums, for this reason, allow weak forces between small objects to be measured, even in the presence of strong forces such as earth's gravitational field. If the system is perfectly calibrated and balanced, then the pendulum is sensitive only to motions caused by the fiber, such as coarsely adjusting the position of the pendulum. This means that as the fiber moves, the pendulum should not rock back and forth. Therefore, the pendulum should only rotate in the horizontal plane due to torques induced by charges, or gravitational waves. By placing the pendulum in a pressurized chamber, extremely weak forces that cause torque to the system can be measured, as is done with UW's pendulum. The pendulum is aligned to the

autocollimator detector by using a feedback loop created by graduate students. Many torsion pendulums use this negative proportional feedback to reduce noise and disturbances to the pendulum. If the feedback is large, the amplification of the motion of the pendulum is mostly dependent on the feedback network. By using a feedback program, the noise and any transient forces acting on the pendulum are significantly reduced. When the pendulum is on the detector it is said to be “caught”. Once the pendulum is caught, weak forces caused by excess charges can be applied to change the torque on the pendulum [3].

The torsion pendulum at the University of Washington uses two Al electrode plates to charge the pendulum. These electrode plates are positively charged by a UV LED and negatively charged by an electron gun. The photo electric effect is the mechanism in which the pendulum is charged. When photons are incident on a material, usually a material with a high conductivity, their energy is absorbed by the electrons. These electrons are then ejected out of the material, causing what is known as the photo electric effect. The material loses electrons and becomes positively charged. By shining the UV LED directly on the Al electrode plate, electrons are ejected from the plate, which causes the plate to charge positively and therefore charge the pendulum [4].

To charge the pendulum negatively with the electron gun, an extra step is needed. The electron gun for the UW’s torsion pendulum is made from two isolated sections, an Al cathode and a Cu nozzle, and is shown in figure 1.2.2. The cathode is coated with magnesium which, with a low work function of 3.66 eV, can easily eject electrons. A second UV LED at a wavelength of 330 nm, and powered at 20 mA, is used to eject electrons using the photo electric effect. The nozzle focuses and accelerates these ejected electrons to the electrode and thus charges the pendulum. It does this by negatively biasing the cathode at -6V [4].

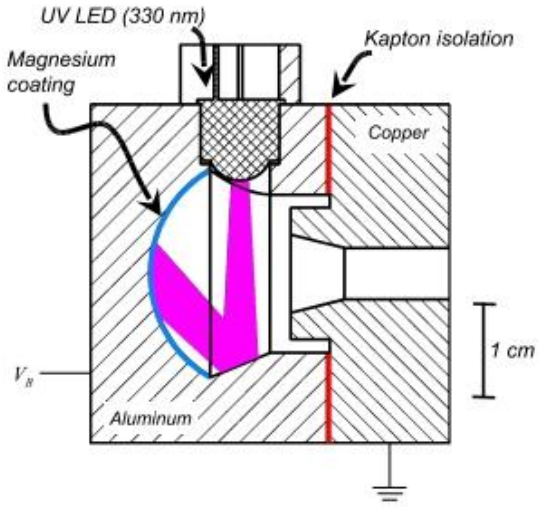

Figure 1.2.2: Cross-sectional drawing of electron gun. Using a UV LED photons are incident on the magnesium cathode and eject electrons through the photo electric effect. When the cathode is biased at -6V, the electrons accelerate to the nozzle and exit the gun to the torsion pendulum and Al electrodes [4].

To improve the electron gun, a design incorporating an Einzel lens was created for this project. An Einzel lens is a system of metal cylinders that take advantage of applied voltages to create an electric field which can pull the ejected electrons through the gun. Figure 1.2.3 is a diagram of the Einzel lens design chosen to optimize the path of ejected electrons from the electron gun. The source potential and the middle lens are placed at the same voltage, and the first and third lenses share a same voltage. By applying a higher voltage to the middle and source lenses, it is possible to create an electric field and pull the ejected electrons from the magnesium plate to the aluminum plate [5].

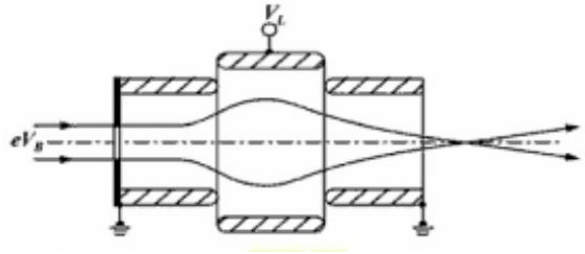

Figure 1.2.3: Einzel Lens. If $V_L = V_b$ then the focal length is twice the diameter of the lens. This design allows the electrons to travel into and out of the lens at the same speed [5].

To measure the differences in path lengths from gravitational waves, LISA uses heterodyne interferometry. Because these gravitational waves come from distant massive objects in space, the accuracy of the length between satellites needs to be greater than what a Michelson interferometer can provide. The Michelson interferometer measures positions of relative fringes, and therefore is not as sensitive as other interferometer alternatives. Heterodyne interferometry replaces the conventional measurements of position of fringes, which correspond to distance, with measurements in the frequency domain which can be measured with much higher precision than position [6,7]. This technique uses one laser source that is separated by a beam splitter creating a reference path and a secondary path. The reference path stays fixed, and the secondary path is allowed to move in position. By moving the position of the secondary path, a frequency shift is created between the paths. When the frequency shifted paths recombine at the end of the apparatus, the frequency shift causes an interference pattern.

The simplified heterodyne interferometer is shown in figure 1.2.6. Using a laser such as a HeNe, the laser beam passes through a Bragg Cell frequency shifter which applies an amplitude division of the beam and allows the position measurements to be transformed into the frequency domain. The reference beam is deflected, at a slight angle, to a stationary mirror

that steers it into the photo detector. The other beam does not change position and passes through the beam splitter to a movable target. The target, in the case of LISA, will be either the proof masses or the torsion pendulum. The beam then reflects off of the target, which by moving causes the relative phase shift from the reference beam, and then finally passes through the beam splitter a second time. Both beams then interfere and recombine into a photo-detector which measures the relative frequency shift between the two beams [7].

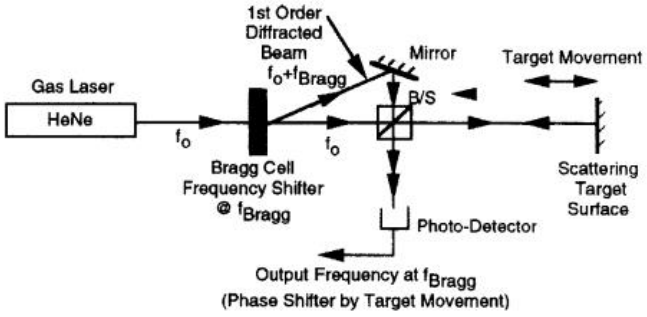

Figure 1.2.4: Illustration of a typical heterodyne interferometer. A laser beam is created and passes through a frequency shifter. This splits the beam which then passes through to a target. By moving the target a phase shift between the two beams is created. This phase shift is measured by a photo-detector as the beams interfere at the end of the experiment [7].

The device that performs this heterodyne interferometery is an autocollimator, shown in figure 1.2.5. This is a specific heterodyne interferometer that incorporates a system of lens to collimate the laser light in the measurements. This autocollimator is designed such that the light stays at 60^o angles to the optical axis, just as the light will be with respect to the sun in space. The autocollimator has a path length of 1 meter, a dynamic range of 1^o, and a noise level of 1 nrad/√Hz, all conditions which satisfy NASA's requirements before making a prototype for space [8]. In the pendulum experiments, the adjustable mirror target in the figure above is replaced with the pendulum which will now act as the movable target.

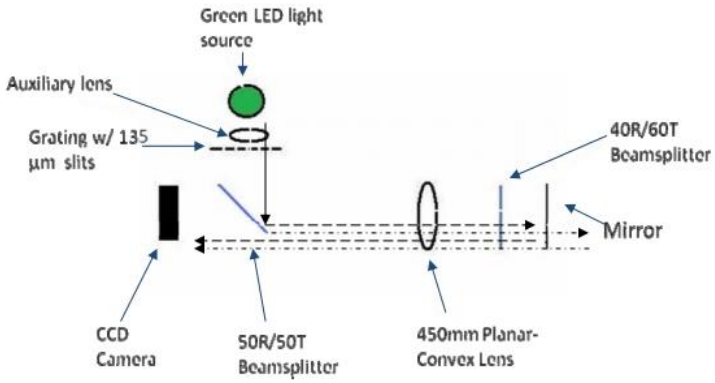

Figure 1.2.5: Illustration of the autocollimator used in the LISA experiments. By passing a beam through a series of lenses, gratings, and beam splitters, a reference beam, whose interference remains stationary on the target and CCD camera, a phase shifted beam is created. Heterodyne interferometry is used to create the interference pattern before being imaged by the CCD camera. Using a DAQ system the relative phase shift between the beams can be measured [8].

2. Experimental Set Up and Data Acquisition

2.1 Charge Control Experiment

The experimental set up for charge control measurements on the LISA satellites involves using a torsion pendulum. This pendulum is designed to be the geometric equivalent of the LISA satellites, as described in section 1.2. The torsion pendulum used was designed by graduate students at the University of Washington. Figure 2.1 is a diagram of the final design used for the charge control measurements.

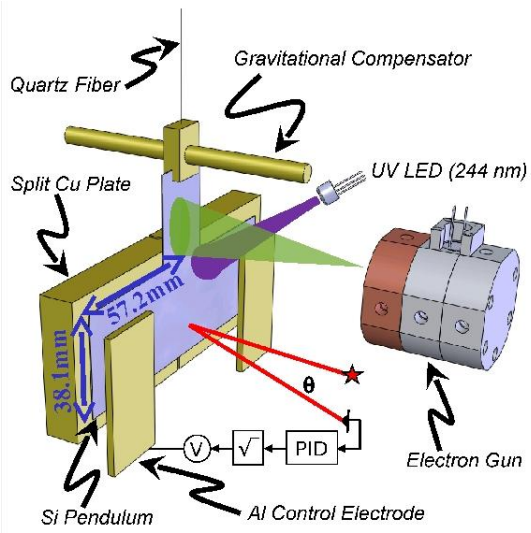

Figure 2.1: A Si torsion pendulum, which is suspended from a thin quartz fiber to a gravitational compensator. It is surrounded by a split Cu plate and two control electrodes. These electrodes are charged by an electron gun and UV LED. By charging the electrodes, a torque is applied to the pendulum. This torque is then measured in degrees (θ) by an autocollimator, as described in section 6.1, represented by the red laser paths [4].

The pendulum is designed to determine forces between the closely spaced conducting proof masses and housing of the three satellites of LISA. The pendulum is suspended from a thin quartz fiber and is made of silicon plate suspended between a copper plate and two conducting

aluminum control electrode plates. To negatively charge the pendulum, an electron gun, with a magnesium cathode, is used. The pendulum is positively charged by using a UV LED at a wavelength of 244 nm, as described in section 1.2. Each is controlled by the LISA DAQ program developed by previous graduate students. The angle of torsion movement, θ, is measured by an autocollimator that uses feeds back, via a proportional-integral derivative (PID) loop, to keep the pendulum angle fixed between the copper plate and the electrodes [4].

The pendulum is housed in a pressurized chamber $3.0*10^{-9}$ Pa and all coarse movements are controlled by a motor attached to the quartz fiber. All other pendulum movements are controlled by charges from the UV LED or electron gun using the LISA DAQ software. Previously no data has been taken incorporating the charging technique and autocollimator measurements to show charge control of the pendulum. Therefore, the first step of this project is to acquire data to demonstrate charge control. To demonstrate charge control, the specifications are that a graph of charging and discharging over time needs to be recorded. The behavior of the graph is decided upon before the experiment is conducted, demonstrating that the pendulum can be charged and discharged in any arbitrary pattern that the user decides upon.

To demonstrate that the pendulum can be charged in any arbitrary pattern, the specifications for this particular experiment were to demonstrate that the user can charge and discharge the pendulum such that the arbitrary behavior of the charge on the pendulum is a sine function over time with a voltage range from approximately -10 V to 10 V. To first acquire data, the pendulum must be “caught” by a detection system, which is controlled by software specially developed by graduate students. To do this, the pendulum is positioned inside the chamber, such that the autocollimator detector can measure the movements. If the pendulum is “uncaught” then it is either swinging outside the range of the detector or the angle of the

pendulum is displaced enough that the motor must be used to drastically change the angle. By using the PID feedback loop, the detector can measure how much the pendulum must be charged to move it directly on the detector. Next, the UV LED or electron gun can be used to negatively or positively charge the pendulum and demonstrate charge control.

One specific feature of UW's torsion pendulum is the use of two Al control electrodes. The pendulum is charged from the charge on the electrodes from the UV LED and electron gun. The UV LED and electron gun cause excess charges to occur on the electrodes, which is then transferred to the pendulum itself. This ensures that the charges measured in the experiment are of the pendulum and not the electrodes or UV LED and electron gun themselves. At specified intervals the "polarity" of the experiment is changed. This means that at specified time intervals the electron gun or UV LED charges the left or right plate and then switches. By charging this way, the experiment ensures that the charges measured are from the pendulum and not electrodes because the charge measured does not depend on the "polarity" of the experiment, or therefore which electrode is used.

2.2 New Electron Gun and Photocurrent Measurements

A new electron gun also needed to be designed for LISA in an attempt to improve the charge control and photocurrent produced from the UV LED exciting the magnesium cathode, as described in section 1.2. The specifications for the electron gun are that the inner radius needs to be 1 inch in diameter and no more than 5 inches tall. The electron gun is made from a hollow aluminum cylinder and cap with a hole for the UV LED to be directed towards the cathode and is shown in figure 2.2. The magnesium cathode is insulated from the aluminum cylinder so that no shorts occur when the aluminum anode and magnesium cathode are set to a different voltages.

Magnesium is chosen for its low work function, and compatibility inside a pressurized chamber such that the magnesium would not spark or react harshly inside the chamber.

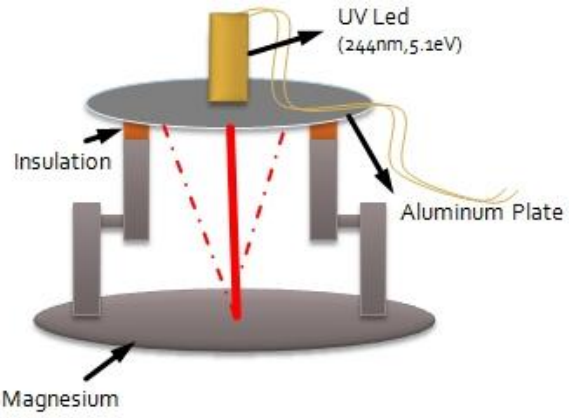

Figure 2.2: Electron gun design to measure photocurrent of UV LED. The cathode is located at the base of the gun and is made of magnesium. The remaining material is made of aluminum and is insulated using plastic insulation from the magnesium. A hole in the top of the gun allows a UV LED to sit in it such that it can directly point to the cathode. The emitted electrons then excite the lid and surrounding aluminum and this induced charge is measured on an ammeter.

To power the UV LED, a custom battery design needed to be made in order to reduce current leakage between the power going to the UV LED and the power going to all the other components of the gun. The design needed to have an adjustable power and current output to the system and no more than a current of 30 mA. Figure 2.3 is the schematic of the battery system. The system is composed of a chip, to control the current, and a system of resistors, variable resistors, and two 9 V batteries to power the UV LED. The variable resistor is used to precisely control the amount of current being supplied and can be adjusted by the user.

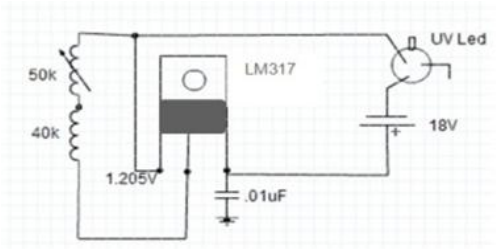

Figure 2.3: Circuit diagram of battery design used to power the UV LED. This design uses two 9 V batteries as the power supply. Two resistors that total 40 kΩ to 90 kΩ are used to control the amount of current passed to the electron gun. A current chip is then introduced to regulate and stabilize the current from the batteries. This battery system is then connected to the UV LED.

The photocurrent of the LED was determined by grounding the magnesium plate and measuring the current and voltage on the cylinder and lid inside a chamber with a pico-ammeter. Trial one was with the UV LED turned off to measure the current from just the battery system, and the subsequent trials were done with the UV LED on. Later in the experiments, a photocurrent DAQ program was designed so as to eliminate background currents. One major source of background noise was the presence of anyone in the room. As someone approaches the system, it is enough to drastically change the current measured, which is on the order of pA to nA. This software was designed to electronically turn the battery system on and off at designated time intervals. Within these intervals, the software measures the current and voltage of the aluminum, which is analyzed to determine if any photo current was produced from the system.

This project also incorporated designing a second electron gun to see if adding an Einzel lens could improve photocurrent measurements, as described in section 1.2. The same data procedure, for the previous design, is used, but the Einzel lens is designed to focus the photocurrent from the UV LED only onto the aluminum plate. It also reduces scattering so that a larger number of electrons could reach the plate. Figure 2.4 shows the Einzel lens design used in

the measurements. The lens was made of three aluminum cylinders. The top and bottom have the same 1 inch diameter as the electron gun and the same length. The middle cylinder is designed to be 0.9 inches, in diameter, such that the Einzel lens is correctly proportioned, as described in section 1.2.

The specific design of the Einzel lens is to direct the electrons more uniformly to the end of the gun where the charge of the aluminum plate is measured. The UV LED is placed at an angle at the side so that the light goes through the electron gun first, and then the lens, making sure that the incident light it is not inside the lens itself, which could cause aberrations in the measurements. This angle is designed to be ~30^{o} so that the UV LED was incident on the magnesium plate, and not the side of the aluminum cylinder.

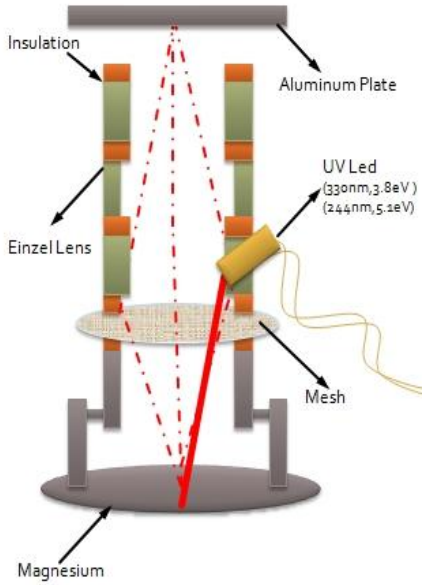

Figure 2.4: Electron gun design with Einzel lens to measure photocurrent of the UV LED. The set up of the electron gun is the same as figure 2.2 however the aluminum lid is now replaced by aluminum mesh, and the UV LED passes through the Einzel lens first.

2.3 Autocollimator Measurements

The autocollimator is used to measure the relative change in the angle or torque of the pendulum as charges are introduced on the system and cause the pendulum to move, as described in section 1.2. Redesign of the autocollimator is an important step for the LISA project before the final prototype can be submitted to NASA. Figure 2.5 is a picture of the autocollimator designed by the previous REU student on the LISA project. A laser beam passes through a diffraction grating and is split into a reference beam and a beam that uses the pendulum as the variable target, as described in section 1.2. The frequency shift of the two beams is read by the autocollimator DAQ software also designed by the previous REU student [8].

The laser source is a green 530 nm LED that passes through a grating with 135 µm slits by a 50 mm PCX lens (auxiliary lens). It then passes through a series of beam splitters and lenses. The image from the reference frame remains stationary while the second path is dependent on the pendulum movement, and is measured by using a CCD camera [8].

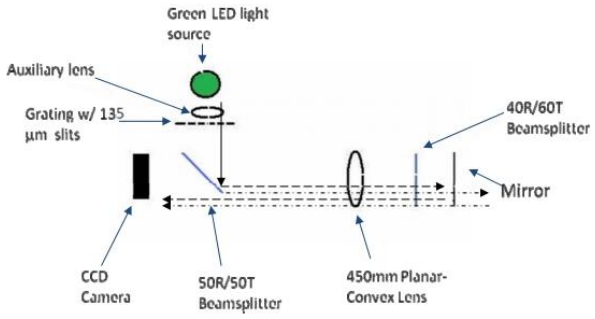

Figure 2.5: Autocollimator design from a previous REU student. The collimator uses a diffraction grating to create two separate beam paths from a laser source. One path is fixed and is the reference beam. The other beam is free to move by adjusting the large lens and associating mirror. Then difference in these two beams is then measured. This technique is used to measure changes in the torsion pendulum by having this reference and movable beam such that any displacement can be detected [8].

For this project, a system of thermometers also needed to be designed to measure any thermal noise that affects the sensitivity of the autocollimator. In a vacuum, or in space, the temperature will not fluctuate as drastically as it will in a variable heated room, and, therefore, one cause of noise of the system is hypothesized to be thermal noise. One thermometer is placed inside the shielded autocollimator and one outside to measure the background thermal noise of each area. By having the second thermometer outside the system an additional experiment can be conducted to see if the system itself is the cause of the thermal noise. Figure 2.6 is the circuit diagram of the thermometer system. The thermometers are powered by a chip connected to the DAQ system and the power goes through an amplifying circuit. Using this particular combination of resistances, the output to the DAQ is on the order of 20 mA, which then is converted by the DAQ system into a temperature measurement in degrees Celsius.

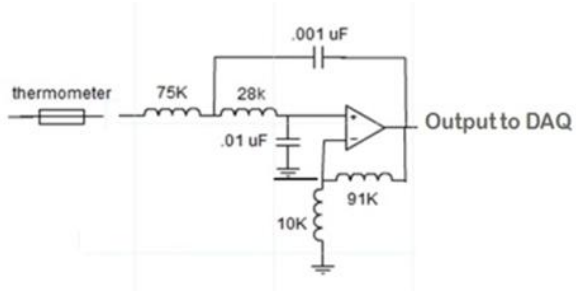

Figure 2.6: Circuit diagram of thermometer system for the autocollimator. Each thermometer is connected to an amplifying circuit and read by a DAQ on a computer. The amplifying circuit uses various resistors and capacitors calculated such that the temperature read by the DAQ is as close to the room temperature as possible.

3. Results and Analysis

3.1 Charge control Measurements of Torsion Pendulum

To demonstrate charge control on the pendulum, and the proof masses of LISA, the pendulum was charged negatively, using and electron, and positively, using a UV LED, from 10 V to -10 V, at a current of 0.1 A. The pendulum was charged for approximately 29 minutes and the data is plotted in figure 3.1. The behavior was arbitrarily chosen as a sinusoidal function to demonstrate that the user could charge and discharge the pendulum in any arbitrary behavior. The pendulum feedback was set to a small value of 0.01 to keep the pendulum on the detector. When the UV LED was on, the duty was set to 10%. This means that for every second the UV LED is on, it is only on for 10% of the time, but in even intervals such that it flashes. When the electron gun is on, the duty was set to 40%.

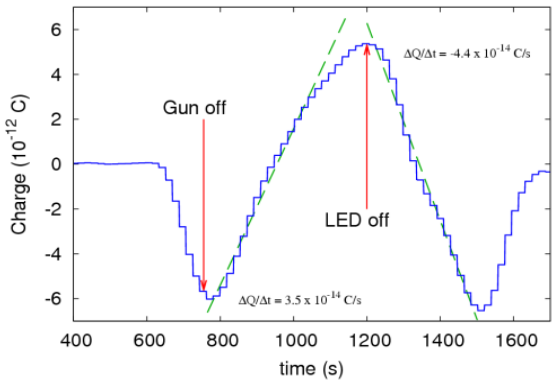

Figure 3.1: Demonstration of charge control. As the electron gun and UV LED are turned on and off the user is able to control the change in charge of the pendulum which is on the order of 0.01 A and a current of -10 V to 10 V.

The pendulum starts at a charge of 0 V. Each data point is taken at 20 second intervals, which accounts for the steps in the data, rather than a smooth curve. By changing the recording

time, this data becomes smoother at shorter time intervals. However, at too small of time intervals, the recording software cannot handle the rapid data being processed. At 650 seconds, the electron gun is turned on to negatively charge the pendulum. At 800 seconds the UV LED is turned on and the pendulum begins to charge until, at 1,200 seconds, the UV LED is turned off and electron gun turned on again. At 1,500 seconds, the UV LED is turned on to return the charge back to 0 V.

Using a program written in gnuplot by previous graduate students, the charge is converted from voltage to current using equation 3.1. This is the capacitance equation, and equation 3.2 defines the capacitance for the pendulum.

$$Q = C * V \tag{3.1}$$

$$C = \varepsilon_0 \frac{A}{d} \tag{3.2}$$

Q is the charge in coulombs, C is the capacitance, V is the voltage measured, A is the area of the pendulum, and d is the length of the pendulum.

The slopes of the charging and discharging are measured to analyze the speed at which the pendulum is charged. The slope of the charging is $3.5 * 10^{-14}$ Cs^{-1}, and discharging is $-6.4 * 10^{-14}$ Cs^{-1}. These speeds may seem quite slow. However, because the pendulum can be charged to as low as 10^{-14} C in a second, this demonstrates the fineness to which the charge can be controlled. Based on the physical restraints of the system, such as the response time of the UV LED and electron gun being turned on and off, any speeds faster than this will be too small for the system to process and therefore the precision in the charge measurements will be lost.

Because LISA is detecting gravity waves with strains *h* on the order of 10^{-21}, any small excess amount of charge could cause noise in the system and greatly affect the outcome of the

results. It is estimated that solar charges could affect LISA at a range from 0.1 eV to 100 GeV. [14] Therefore precise control over the charges induced on LISA from the electron gun and UV LED to cancel out this charge is extremely important. Therefore the speed of charging at 10^{-14} Cs^{-1} allows for the masses and pendulum to obtain this fine control. The precision to which the charge is measured by the autocollimator is also a success. The charge on the pendulum can be measured to within a few pC, which will allow the charge of the pendulum to be very finely controlled.

The behavior of the data from the charge control experiment also behaved as was defined by the specifications of the experiment. The shape of the graph is arbitrarily chosen by the user to be sinusoidal, and, because the sinusoidal shape could be produced by the user, demonstrates charge control of the pendulum.

3.2 Photocurrent Measurements with New electron gun

3.2.1 Simple Design

To improve LISA and characterize the output of the UV LED that runs the electron gun, a new design was made. The specifications are that the body of the gun should be made from aluminum and the cathode from magnesium as is shown in figure 2.2. The gun is made from an aluminum cylinder 3 inches high, and 1.5 inches wide with a inner diameter of 1 inch. It is secured by an aluminum ring and insulated from a magnesium cathode plate, whose diameter only needs to be bigger than that of the cylinder. The cylinder is then capped with an Al lid which is approximately 0.5 inches thick. The size of the gun was decided upon such that the UV LED could fit on the lid and that all the light from the UV LED is incident on the cathode only. Also, the size allowed for the electron gun to be made with machinery, such as a lave and mill

machine. All parts were fabricated with high precision tools such that the diameters and specifications were uniform throughout the gun.

To test the prototype for the electron gun, it was placed inside a pressurized chamber, at $3.9*10^{-9}$ Pa, to replicate the pendulum's environment. Leads in the chamber, which connect electrical components inside and outside the chamber, were used. A lead was connected to the magnesium and was set to ground using the power supply, such that all measurements were grounded with respect to the cathode. The aluminum lid was then connected to a separate lead connected to an ammeter to measure the photocurrent of the electron gun, see figure 2.2 in section 2.2. The cylinder was then charged at various voltages to produce photocurrent in the system from the UV LED. Figure 3.2.1 is the photocurrent measured from the electron gun from voltages of -6 V to 6 V. The blue data points indicate that the UV LED is turned off, and therefore is the background current of the gun. The red data points are when the UV LED is on. Taking the difference of these two data sets should produce the photocurrent of the system.

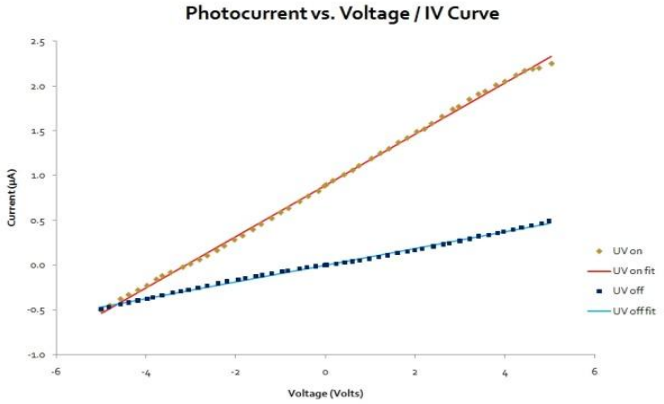

Figure 3.2.1: Photocurrent measurement from electron gun design (figure 2.2). The blue data set is without the UV LED turned on and the red is with the UV LED on. The difference between these data sets should yield the photocurrent. However, with more investigation, it was found that this was a false reading, and the increase in current was current leakage from the power supply turning the UV LED on, and not that of the photocurrent produced by the UV LED itself.

However, with more investigation, it was found that the photocurrent that was measured was a false reading. The data was actually the current caused by current leakage from the power supply running the UV LED. This was discovered by taking out the electron gun from the chamber and measuring the current leakage from only the UV LED in the chamber. As can be seen, this current leakage greatly affects the data, and causes the user to think that they are measuring photocurrent, when this is not the case. To fix this issue, a new battery system was designed to power the UV LED separately from the rest of the electron gun. The design is shown in figure 2.3 in section 2.2. The UV Led is powered by two 9 V batteries that are connected to an amplifying circuit fabricated on a bread board. By using a 40 kΩ resistor in parallel with an adjustable 50 kΩ resistor, the current has a range of 0 mA to 30 mA. This was calculated using Ohm's law and measuring the direct current from the batteries themselves. The design also incorporated adding an amplifying current chip, LM317, with a 1 µF capacitor, creating a negative feedback loop that could better control the stability of the current. By adding this separate power supply the current leakage was significantly reduced.

3.2.3 Einzel lens Design

A second improvement, on top of the separate battery supply for the UV LED, was incorporating an Einzel lens to the electron gun to focus the ejected electrons onto the Al lid. For a simple Einzel lens, the specifications are that the two outer cylinders had smaller inner diameters then the middle cylinder, and that the length of each cylinder is the same. The length of each cylinder was 3 inches to match the length of the original electron gun design. The inner diameter of the outer cylinders was 0.9 inches, and the middle was 1 inch to match the original cylinder. The new design is shown in figure 3.2.2 and was designed with the software

SolidWorks. A hole, the diameter of the UV LED, is placed on the first cylinder at ~30^{o} such that the incident light hits the cathode only as is shown in section 2.2 figure 2.6.

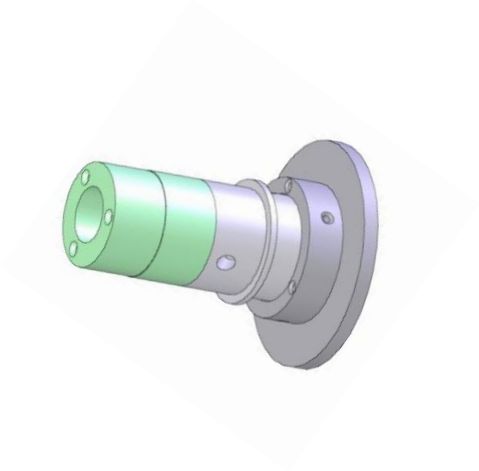

Figure 3.2.2: Electron gun design with an Einzel lens using SolidWorks. The inner diameters of the outer cylinders are 0.9 inches and middle is 1 inch. All cylinders are 3 inches in length to preserve the symmetry of the Einzel lens design.

The hope is that by adding this lens, more photocurrent can be measured from the electron gun. Figure 3.2.3 shows the data taken with the Einzel lens design using two different UV LEDs at wavelengths of 244 nm and 330 nm. By using two different wavelengths, the measured photocurrents should be different since they will produce different electron energies. Therefore, because these energies are different, the photocurrent measured should be different. The outer cylinders at the same voltage, and differ by one volt from the inner cylinder and Al cylinder. The middle cylinder and original Al cylinder are placed at a different voltage from that of the outer cylinder pair. The voltage recorded in figure 3.2.3 is the voltage on the middle and Al cylinders. The photocurrent is found by taking current readings from -10 V to 15 V with the UV LED on and off. The photocurrent is then the difference of these two data sets.

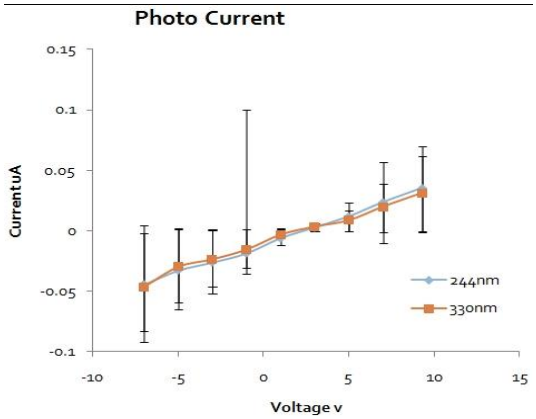

Figure 3.2.3: Photocurrent measurements from the Einzel lens design. The orange data is with a 330 nm UV LED and the blue data with a 244 nm UV LED. By using different wavelengths the photocurrent measured should change. However from the data, it can be seen that this is not the case.

Figure 3.2.3 shows that there is no significant change in photocurrent from either UV LED. This means that there are two possibilities. The first is that there are still flaws in the system, such as additional current leakages, which are causing significant noise in the system. The other possibility is that the photocurrent produced by the electron gun is too small for the pico-ammeter to detect. In section 3.1 it was seen that the charge on the pendulum only differed by a magnitude of order of 10^{-12} A, which would correspond to a significantly small current as well. Therefore the measurements may be too small to be measured with this setup. The obvious disadvantage of this scenario is that the photocurrent, and therefore efficiency of this new design, cannot be measured, which means there is not a way, at this time, to tell if this design will improve the LISA pendulum. However, an advantage is that this setup is producing such fine changes in current that it cannot be measured. This is an advantage because, once a way to measure this current is found, the current can be controlled to very precise values which would only improve the functionality of LISA.

3.2.4 Final Measurements and Conclusions

The final improvement, made to the electron gun thus far, was to incorporate a computer control system that could run the electron gun without the presence of the user in the room. It was observed that if a person is in the room as the experiment is being conducted, they are producing a current leakage themselves, and by walking around the room they can change the current readings from the ammeter. To eliminate this issue the LISA adviser, Stephan Slamminger, quickly programmed a control system using C++ that could run the experiment from a remote desktop in a separate room. The software was programmed based on specifications given by this author, on how to improve and measure the current. First, the UV LED battery needed to be turned on and off at designated time intervals defined by the user, which means that only one voltage per run can be measured. Secondly, at these intervals, the current of the electron gun needed to be measured. Figure 3.2.4 is the output of the program during one trial of the experiment. The red data indicates the current of the UV LED, and if the UV LED is on or off. The green data is the corresponding currents measured at these time intervals.

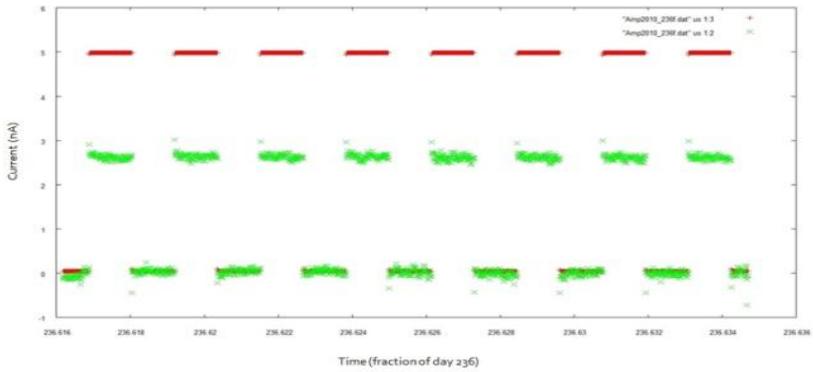

Figure 3.2.4: Photocurrent measurements using DAQ softeware to remotely run the experiment. The red data is the current supplied to the UV LED which indicates when the UV LED is on or off. The green data is the photocurrent measured during these same time intervals.

The data above seems to indicate that when the UV LED is turned on photocurrent is produced from the gun at approximately 2.7 nA. This seems promising, but further experiments were done to determine if this, again, was a false reading, or if the current measured was really from the photocurrent produced by the gun. To test this, the current was measured using the DAQ system above, but at various voltages applied to the Al cylinder. Figure 3.2.5 shows the data that was obtained. The current rises as a function of voltage and then asymptotically approaches a final current. This is indicative of photocurrent and the photo electric effect. Therefore this seems to verify that photocurrent is being measured from the gun.

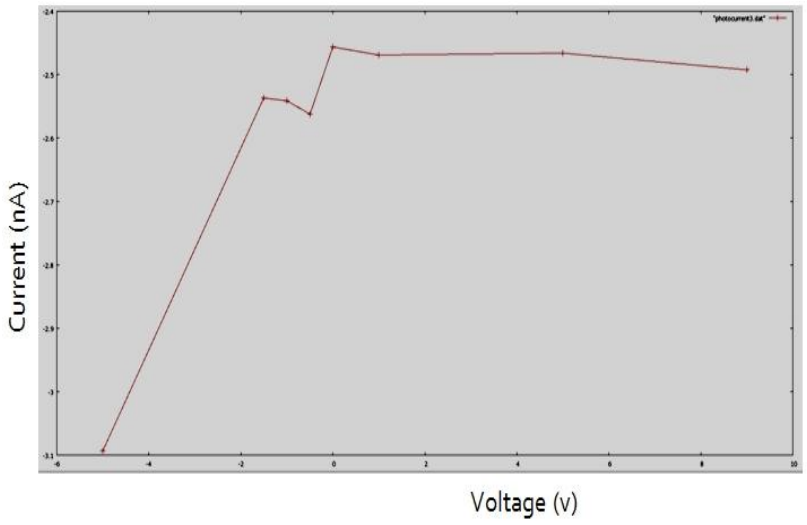

Figure 3.2.5: Photocurrent measured from electron gun design using the DAQ software. Each data point is taken at different applied voltages to the Al cylinder. The behavior of the graph is indicative that photocurrent is being produced in the electron gun and can be measured.

One final run was done to determine if this is definitively photocurrent that was being measured. Pieces of the system that were physically moveable, such as the batteries, were moved around during the DAQ trial run to determine position effects on the photocurrent

readings. Figure 3.2.6 shows data taken as the batteries going to the UV LED were wiggled in place.

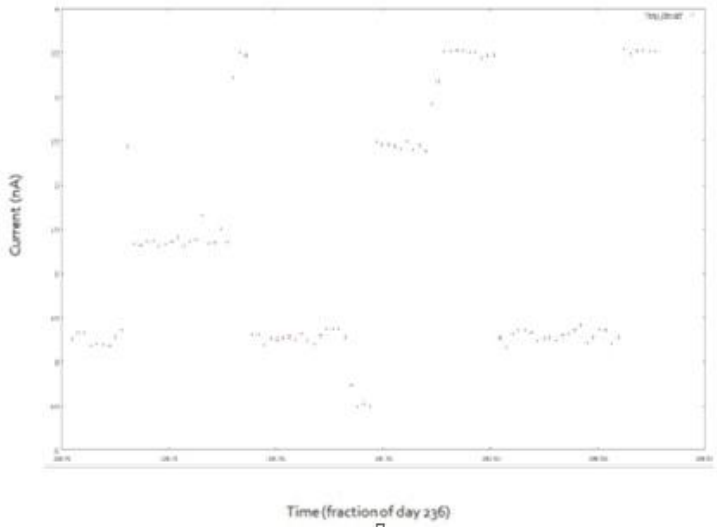

Figure 3.2.6: Photocurrent measured from electron gun design using the DAQ software. The batteries powering the UV LED are physically moved by the user to demonstrate that the change in position of the battery causes a change in the current measured.

The data above shows that the current can be affected by the movement of the battery. Therefore this may indicate that all of the previous data may have been false readings. However, this cannot be concluded one way or another. Unfortunately, due to time constraints of the REU program, more trials could not be conducted to definitively address this problem. However, some conclusions can be drawn from this data which will need to be tested at a later date.

Because the photocurrent produced is significantly small, it is hard to conclude whether the current measured was really photocurrent. There are too many factors that could contribute significant noise to the system and create misleading data, such as the current leakage

described above. The hope is that this photocurrent is real, and that by cutting down on noises, such as fixing the position of the battery so that it cannot move, the photocurrent can be measured.

It is believed that the current measured is false, and that the photocurrent is so small that with the measurement tools available there is too much noise to distinguish the real photocurrent from the measurements. Even though photocurrent was not measured as was hoped, this does not mean that all of this work was done in vain, but that significant progress was made in determining the mechanical limits and capabilities of the electron gun, and improvements that must be made before a NASA prototype can be built. As stated before, this setup is producing such fine changes in the current that the current cannot be detected. However, once a way to measure this current is found, the current can be controlled to very precise values which would only improve the functionality of LISA itself. Once a way to measure the photocurrent from the new electron gun design can be fabricated, then characterization of the gun and UV LED can be conducted to determine whether this simple design can suffice for the final LISA experiment.

3.3 Thermometer and Autocollimator Measurements

Another improvement on the LISA pendulum is the noise control of the autocollimator designed by the previous REU student. Figure 3.3.1 shows one of the most recent data runs of the autocollimator for LISA. The goal of autocollimator is to be sensitive enough to changes of 10^{-9} rad $Hz^{-1/2}$ in the position of the pendulum.

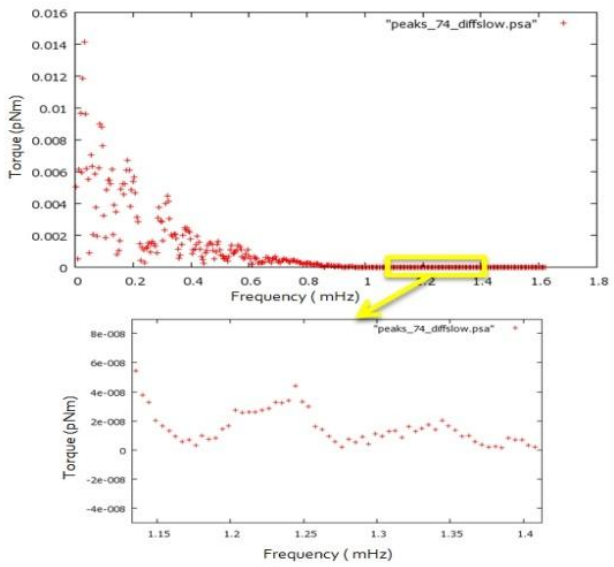

Figure 3.3.1: LISA autocollimator data. It is observed that the sensitivity is only ~10^{-8} rad $Hz^{-1/2}$ where the sensitivity goal is 10^{-9} rad $Hz^{-1/2}$.

The data shows that the sensitivity of the autocollimator is fairly good, and is about 10^{-8} rad $Hz^{-1/2}$. This means that the sensitivity of the autocollimator needs to be improved by an order of magnitude. It is hypothesized that this can be done by finding thermal noise of the system and trying to reduce it. The first step in incorporating a thermal noise detector into the autocollimator is to first build a thermometer device that can measure the source of thermal noise, and the extent to which it is affecting the measurements.

In section 2.2, figure 2.6 shows the circuit diagram for the thermometer system. This design was created on a bread board and designed to measure the temperature inside the housed autocollimator and the outside environment. Therefore two thermometers were built using figure 2.6. The thermometer, made by a commercial manufacturer, is connected to a negative feedback amplifying circuit. By using the combination of resistors and capacitors, and by using Ohm's law and other fundamental electronic equations, the output of the circuit

produces an output of approximately 20 mV. The specifications of the thermometer state that an output reading of 1 mV corresponds to a temperature change of 1 ^{o}C. Therefore a reading of 20 mV is approximately 20 ^{o}C, which is around room temperature.

To obtain an accurate reading of the thermal noise, the thermometer system needed to be calibrated. The thermometer system was calibrated by using an oven at a known temperature. The thermometers were placed inside the oven and the outputs were recorded in figure 3.3.2. The output readings were converted from mV to ^{o}C and described above.

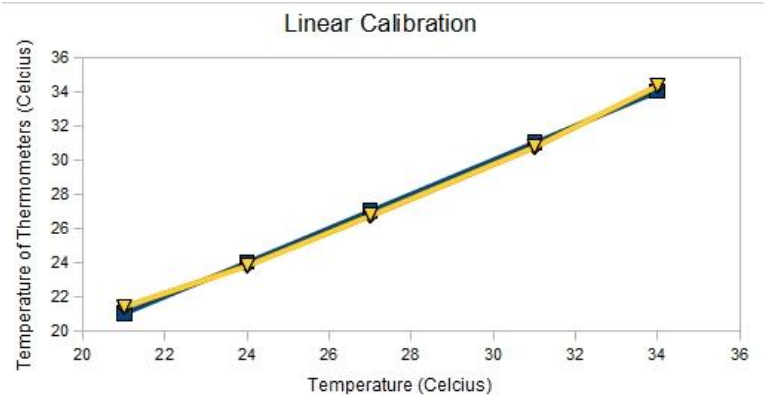

Figure 3.3.2: Calibration of output temperature readings from thermometers versus actual temperature of the surrounding environment. Using the linear component of the plot the output temperature can be calibrated in the DAQ system.

By plotting the temperatures read by the thermometer, with the actual temperature of the oven, the output can be changed using an algorithm in the DAQ software, such that the mV read is the same number of ^{o}C as the environment. To change the output of the thermometer outside and inside the box, the linear fits to the calibration curves are used. These equations are the linear components of the above graph since the temperature and voltage should behave

approximately linear.

Once the thermometers were calibrated, temperature measurements were taken inside and outside the box. Figure 3.3.3 is temperature data inside the autocollimator system with foam shielding. Data was taken for approximately 18 minutes while no one was in the room.

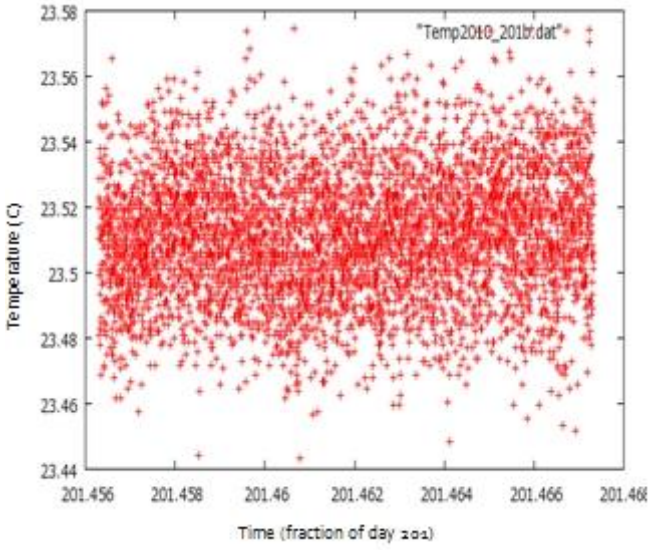

Figure 3.3.3: Temperature data taken from the inside of the autocollimator in foam shielding. The temperature fluctuates by 0.14°C which indicates thermal noise that may contribute a significant amount of noise to the autocollimator measurements.

This data shows that the temperature inside the autocollimator fluctuates rapidly from 23.44°C to 23.58°C. In everyday experiences this temperature difference is insignificant. However, the noise of the autocollimator only needs to be improved from 10^{-8} rad $Hz^{-1/2}$ to 10^{-9} rad $Hz^{-1/2}$, and therefore this small change in temperature may be enough to contribute this last correction to the percentage of noise to the system. Again, due to time constraints, a solution to this thermal noise was not pursued. However if the system was housed in a more stably thermal enclosure the sensitivity of the autocollimator will be improved, and possibly by the order of

magnitude needed. Even though the thermal noise has not been quenched, the measuring devices needed to measure thermal noise were fabricated, and the data did show that there was significant thermal noise. Further experiments will be needed to determine whether or not the thermal noise will improve the sensitivity by the order of magnitude needed. With the thermometers and a more stable thermal environment, a fairly quick and simple experiment can be conducted to see if the desired sensitivity can now be reached.

4. Conclusion

The purpose of this project was to fabricate and test various improvements to the LISA torsion pendulum experiments at the University of Washington in preparation for their final NASA prototype. The purpose of the pendulum is to cancel out any solar charges in space that can cause unwanted torque on the test masses. Charge control measurements were paramount to showing that the system could be used to do this. By producing and arbitrary sinusoidal behavior of the charge on the pendulum, this charge control was obtained. The charge can be changed by increments as small as a pico-coulomb. The average charging for the UV LED is $3.5*10^{-14}$ C/s, and electron gun is $-4.4*10^{-14}$ C/s. This allows for very precise control which allows precision for the LISA prototype.

A new electron gun design also was to improve the prototype. By fabricating two different electron guns made of aluminum and magnesium, one with an Einzel lens and one without, the photocurrent of the UV LED was measured. The first set of experiments in figure 3.2.1 seemed to present verification of photocurrent in the system. However, this was discovered to be current leakage in the system. To compensate for this error a battery system, figure 2.3, was built and subsequent results, see figure 3.2.3, showed that no difference in current was obtained from using two different wavelengths for the UV LED, and therefore no photocurrent is being produced, or is too small to be measured by the ammeter.

The final improvement was to incorporate a DAQ system to electronically control the system. As the voltage is turned on and off the current increases accordingly and seems to indicate photocurrent. The voltage was then varied and current measured in figure 3.2.5 in which the behavior linearly increases and asymptotically approaches a maximum current, as would be expected in the photocurrent measurements. However, it was discovered that by

moving the battery system, the current jumps drastically. This leads to the final conclusion that the photocurrent measured before may not be photocurrent and therefore the results of this project are inconclusive.

Finally, the autocollimator used to measure the torque on the pendulum using heterodyne interferometry was improved by investigating thermal noise in the system. A system of thermometers, see figure 2.6, was fabricated to measure the temperature inside and outside the autocollimating system. Data in figure 3.3.3 confirms that there were temperature fluctuations in the system. This fluctuation is 0.14 ^{o}C. The autocollimator measurements need to be improved by an order of magnitude and this temperature fluctuation is hypothesized to be enough to account for this error.

Unfortunately, time constraints on this project did not allow for enough time to make the necessary improvements to this project and further experiments that were needed to find conclusive results. Future experiments must be done to vary the voltage between the Mg and Al of the electron gun and take photo current measurements to show that photocurrent was being produced. The battery system needs to be bolted down and the connections more secure such that the system can be moved without changing the current. A more sensitive ammetter may also need to be used because the photocurrent may be too small for the current technique to measure. Once the photocurrent can be conclusively measured, full test of the electron gun with the Einzel lens can be conducted. This is the final design for the electron gun system for the pendulum so extensive tests needed to be conducted to show that it works correctly.

As for the autocollimator, the autocollimator and temperature programs are to be integrated so they can be correlated at the same times and specific fluctuations can be mapped onto the autocollimator data. The final goal is that, with all these improvements, the

autocollimator can be redesigned and incorporated into the system such that a final prototype for NASA can be fabricated and delivered.

5. Acknowledgments

A special thanks is in order for the Institute of Nuclear Theory at the University of Washington for providing the summer REU experience needed to conduct this research, and to NSF for funding this opportunity. Thank you to the REU staff Alejandro Garcia, Deep Gupta, Janine Nemerever, and Linda Vilett for making this possible. Thanks goes out to my advisors Stephan Schlamminger (UW) and Oksana Ostroverkhova (OSU) for helping me with my project and reviewing my thesis. Thanks also goes out to Charlie Hagedorn, Jens Gundlach, David Hyde, Ton Musgrave, Etowah group members, and 2010 class of the summer REU for helping me with all aspects of my project including designing, fabrication in the machine shop, and emotional support.

I would also like to thank the 2011 senior class in physics at OSU for revising and helping me do edits on my thesis. A big thanks also goes out to my senior thesis teacher Janet Tate for helping us plan out and efficiently going about the thesis, and for being generous to make corrections to the thesis which only improved its quality. Finally, a special thanks goes out to my boyfriend, Daniel Gruss, who supported my decision to go to the REU at UW and for helping me work through some design and computational aspects of my project.`

I would also like to that the National Science Foundation for funding this REU program and NASA and ESA for funding LISA experiments and opportunities at the University of Washington.

Bibliography

[1] D.A. Shaddock, “An Overview of the Laser Interferometer Space Antenna,”Astronomical Society of Australia **26**(2) 128-132 (2009).

[2] “Relativity,” MaGraw-Hill *Encyclopedia* Fig.3 (2011) <http://accesscience.com>

[3] G.T. Gillies and R.C. Ritter, “Torsion Balances, Torsion Pensulums, and Related Devices,” Rev. Sci. Instrum. **64**, 283 (1993).

[4] S.E. Pollack, et al., “Charge Measurements for Gravitational Wave Observatories using UV LEDs,” Phys. Rev. D 81, 02110(R) (2010)

[5] H. Liebel, Applied Charged Particle Optics 39-43 (Springer, Verlag Berlin Heidelberg New York), 2008.

[6] P. Hariharan, Optical Interferometry **2** 95-96 (Elsevier Science, San Diego, CA), 2003.

[7] W. Boyes, Instrumentation Reference Book **4** 194-195 (Elsevier Science, Burlington, MA), 2010.

[8] J. Walrath, “LISA Autocollimator,” Unpublished manuscript, Institute for Nuclear Theory Summer REU 2009, University of Washington (Seattle, WA), 2009. <http://www.int.washington.edu/REU/2009/2009_images/WalrathPaper.pdf>.

“Lab on a Chip” project

6. Introduction

The Photonics and Electronics Laboratory at Oregon State University is developing a “Lab on a Chip” microfluidic device to aid biologists in the study of cell responses to different ion environments. This project is funded by the ONAMI grant entitled *Biochemical Sensors and Integrated Measurement Platform Controlled by Optical Tweezers and Microfluidics*. The overall goal of this project is to simultaneously optically trap and excite fluorescence of nano-sensors that can be placed inside of cells housed in microfluidic channels. The sensors are then used to track cell changes due to ion gradients introduced into the channel. As different environments interact with the cells, the cells can deteriorate, mutate, or change in various ways due to the chemical responses in the cell. With this instrumentation, biologists could study the effects of ion gradients on healthy, cancerous, and other cells to learn more about how they respond. With this information, for instance, better medical treatments can be developed and given to cancer patients to treat or even cure the cell mutations.

Today intracellular measurements are becoming a collaborative research opportunity between major fields of science including chemistry, biology, and physics, with a goal of obtaining further information and understanding about physical and chemical processes within a cell. As for the nano-sensors themselves, by optically trapping them and using fluorescence spectroscopy, the goal is to use them as measurement probes within a cell [9].

Thus far, a design of the procedure, to optically trap and image nano-particles with optical tweezer trapping, and conduct fluorescence spectroscopy measurements, was needed to

be developed such that the instrumentation could eventually be used intracellular measurements. Thusly, a proof-of-concept of these measurements has been conducted with and without the microfluidic devices using commercial Fluorospheres for this particular experiment. This is done because their fluorescence is well known, and therefore, if the instrumentation and measurements produce the correct fluorescence of these particles, then the experimental set up has been built correctly. Once this is done, newly developed nano-sensors can replace the Fluorospheres in these experiments and characterization of the sensors can be conducted.

This project incorporates the fabrication of nano-particle sensors, fabrication of the microfluidic channels, design of the instrumentation, and collaborative research between the physics and chemistry departments. With the development of the "lab on a chip", biologists can experiment on a variety of cells. Unlike cellular research today that can only measures changes in cells, the nano-sensors are designed to be implanted into the cell itself such that the ion gradient inside the cell can be precisely measured. Figure 6.1 shows an embryonic cell into which K^+ ion nano-sensors been successfully injected to observe intracellular potassium transients. These sensors are not optically trapped, but the sensors have been introduced and excited in the cell without destroying the cell itself [10].

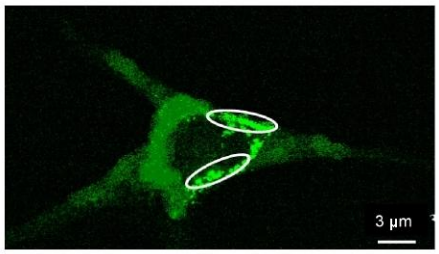

Figure 6.1: An embryonic cell in which K^+ ion nanosensors have been successfully injected into the cell to observed intracellular potassium gradients [10].

To trap the sensors, optical tweezers are needed in the instrumentation being developed. Optical tweezers work by using forces of radiation pressure from focused laser beams to trap a particle. Optical tweezers usually use an inverted microscope and a lens with a high numerical aperture to focus the light. By having an inverted microscope, which puts the sample after the lens and then measures back scattered light from the sample, the imaging lens itself can achieve the focus needed to trap a particle at micron sized points. Many designs then move the sample, not the laser, to move the trapped particle, to ensure that stability and alignment of the beam is consistent. To achieve trapping, the forces pushing the particle into the laser beam must overcome the forces pushing the particle out [11]:

$$F_{gradient} \geq F_{scattering} + F_{absorption}$$

The gradient force, F_{grad}, comes from the parallel component from the light intensity of the beam, and points toward the maximum intensity region of the beam. This is the force that is caused by tightly focusing the beam. As light passes through a dielectric material the light bends due to the change in index of refraction of the material. The bending of the light causes the gradient force on the particle, which pushes the particle into the beam and traps it [11].

The scattering force, F_{scat}, points in the direction of the incident light and is the radiation force of the scattered light that points away from the beam. The absorption force, F_{abs}, is the force caused by the materials in the particle absorbing the light, and this force points away from the beam as well. Therefore to be trapped, the forces must balance correctly as shown below in figure 6.2. The basics of optical tweezers can be easily understood and can be summed up to just tightly focused light on a particle that causes attractive and repulsive forces on the particle. As longs as the attractive forces are greater the repulsive forces, the particle will be trapped [11].

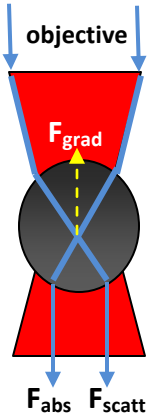

Figure 6.2: Forces acting on a particle (grey) in an optical trap from a tightly focused laser beam (red) such that the forces conserve the property that $F_{gradient} \geq F_{scattering} + F_{absorption}$.

To gain reliable control over the environment surrounding the sensors and cell for the "Lab on a Chip", a microfluidic device is used. A microfluidic device is a network of reservoirs and micron-sized channels that are etched into a surface, for example in a polymer, that create a system where experiments can be conducted *in situ* on the device. The flow, within microfluidic devices, is non-turbulent. To mix the ion into a gradient solution, the channel uses diffusion within the channel. This allows multiple channels to contain different solutions in the device without extended mixing between the different channels. Therefore, many channels can contain different solutions and will only mix when the channels converge into a main channel where the mixing is wanted. This allows the environment to change in a very reliable fashion that can be controlled by the design of the channels based on specifications of *in situ* experiment [9].

7. Experimental Set Up and Data Acquisition Procedure

The experimental set up for the “Lab on a Chip” has yet to be developed, so the bulk of this experiment was to design and test an experimental set that could be used in the final “Lab on a Chip”. The experimental set up involves simultaneously aligning an excitation laser and a trapping laser into a microscope to trap, excite, and measure the fluorescence of the particles, as described in section 4.1. Figure 7.1 is a schematic of the experimental set up. A Ti:Sapphire laser serves as both the excitation source at 532 nm and a trapping source at 800 nm by producing both beams in different optical cavities of the laser assembly. The trapping laser is passed through the objective of the microscope at a power of 5-10 mW. The objective has a high numerical aperture of 1.4. This allows the laser to be tightly focused and capable of trapping small particles such as nano-sensors. The laser is then focused onto the sample where sensors are then trapped. The fluorescence excitation source is a green laser, with a wavelength of 532 nm, at a power from 10-100 μW. The laser is also passed through the objective and is used to excite fluorescence of the nano-sensor. Both these lasers must be focused onto the same spot on the sample within a micron, or smaller, so that a single sensor can be trapped, excited, and measured with a USB 2000 spectrometer, all simultaneously.

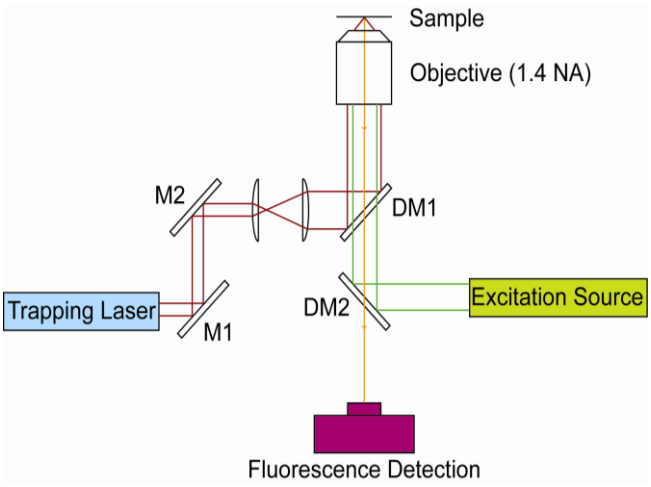

Figure 7.1: Schematic of "Lab on a Chip" experiment. An infrared laser at 800 nm (red) at 5-10 mW is directed into an inverted microscope to trap the sensors using a Ti:Sapphire laser. The objective of the inverted microscope is 1.4 NA to ensure that the numerical aperture is large enough to tightly focus the light onto a nano-particle and thus trap it. Simultaneously, the excitation laser at 532 nm (green) and at 10-100 µW is directed onto the same spot in the microscope such that the trapped sensor is also the sensor being excited. Excitation and trapping are each done in the confocal setting, such that only one sensor at a time is excited and trapped. The output of the microscope (yellow) is connected to a USB 2000 spectrometer and the fluorescence signal from the sensors is recorded using the USB 2000 software package.

The microscope is set in the confocal setting. This means that the laser light from the excitation laser is focused onto a small region of a few 100 nm of the sample. This is opposite from the normal wide field imaging, at which the entire sample area is illuminated. The confocal setting is used so that only one nano-sensor is being excited and trapped at a time. This ensures that all the fluorescence detected is from this one sensor, and protects all the other sensors from photo bleaching.

To measure the fluorescence from the sensors, a fiber optic cable is connected to the confocal port of the microscope and connected to a USB 2000 spectrometer. The confocal port must be aligned at the same point on the sample, as the two lasers, so that the only

fluorescence measured is that from the excited sensor. The fluorescence of the particle can be measured from the sample using the USB 2000 software.

The samples are prepared on a glass cover slip or inside a microfluidic channel. The microfluidic channels are fabricated in the chemistry department at Oregon State University and are made from polycarbonate substrate, in which the channels are etched using a laser, as described in section 4.1 [12].

All preliminary measurements of fluorescence, to demonstrate proof-of-concept of the optical set up, were done on commercial Fluorospheres with well known fluorescence spectra, shown in figure 7.2. Because the nano-sensors themselves are in their experimental phase, any inconsistencies in the fluorescence could affect this proof-of-concept of the experimental set up. However, by using the Fluorospheres first, the experimental set up can be verified. Once the optical set up is correct, the nano-sensors are used and their fluorescence characterized.

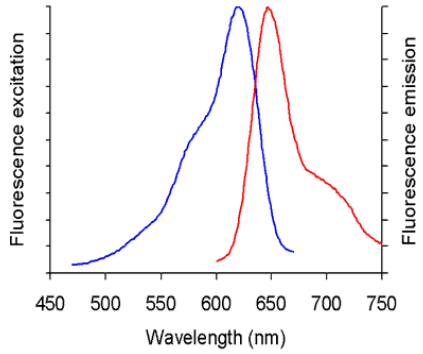

Figure 7.2: Fluorescence spectra of commercial Fluorospheres (provided by the manufacturer) used for proof-of-concept of the experimental set up.

The nano-sensors used for the “lab on a chip” are designed and created by the Chemistry department at Oregon State University. The sensors are optodes which are cation-

selective optical sensing particles that range in size from 1 µm to 10 µm, shown in figure 7.3. They are composed of a plasticized polymer matrix that is integrated with ligand (ionophore, L) that selectively binds an ion target. It also contains an ion exchanger that produces mass transport of ions (R^-) with a protonated pH indicator (chromoionophre, CH^+) [13].

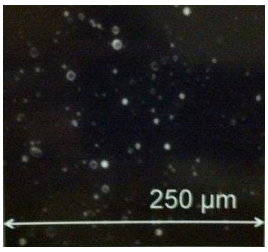

Figure 7.3: Fluorescence image of micron-sensors in solution [13].

When the optode is introduced to an ion gradient, the protonated chromoionophore and ionophore interact with the optode to create fluorescence emission. The optodes change the pH of the environment by having the ionophores interact with the protonated ions, which serve as the reference of the pH. If a solution has the addition, and this case the reference element of H^+, which is not an ion of interest, this is known as protonation. When the ion of interest is absent from the nano-sensor environment, the protonated fluorescence peak dominates since the chromoionophore has no ions to interact with, this characterizes acidic solutions. When the ion heavily concentrates the environment, it interacts with the chromoionophore and produces a fluorescence that is dominated by the deprotonated peak, and this characterizes basic solutions. This interaction is shown in figure 7.4, where an ion K^+ gradient is introduced to the sensors. As the time elapses, a new fluorescence spectrum is taken every 4 seconds as the ion concentration increases. Therefore, the first peak (black) is at time zero and is protonated. As time elapses, the deprotonated (red) peak becomes the dominant peak. These peaks are how the sensors measure changes in the environment, inside or outside

the cell [13].

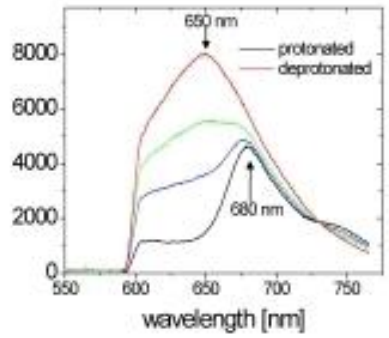

Figure 7.4: Time dependent fluorescence measurements of the nano-optode sensors created by the Oregon State Chemistry Department. Each fluorescence measurement is of the same sensor but at 4 second intervals. As the concentration of the ion of interest increases over time, the deprotonated peaks begin to overcome and dominate the first protonated peak that was, in the beginning, dominate [13].

The microfluidic devices used in this work were fabricated by collaborators in the OSU chemistry department. A diagram of a device is shown in figure 7.5(a), and figure 7.5(b) is an image of an actual device [12]. The preliminary optical measurements were done with devices that were made from polycarbonate and channels created through laser etching. The polycarbonate is bounded to at 170 µm thick glass cover slip. The microfluidics for nano-sensor manufacturing were made from cyclic olefin copolymer. They not only have channels but a "micro-reactor" reservoir, using two stage thermal embossing and bonded with vaporized solvent welding, where the sensors can be made *in situ*[12]. The solutions are added to the device through simple pumps that will push the solution into the channels at one end and help relieve excess solution at the end of the device [12].

(a)

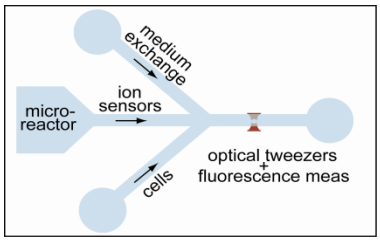

(b)

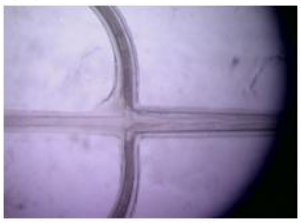

Figure 7.5: (a) Diagram of a microfluidic system. Nano-particle sensors are put into the micro –reactor, ion gradient in the medium exchange, and cells in the cell channel. The three solutions combine in the channel and the nano-particles are then trapped, and fluorescence spectroscopy measurements are be conducted. (b) Actual image of a microfluidic device fabricated by the chemistry department at Oregon State University [12].

8. "Lab on a chip"

8.1.1 Designing the Experimental Setup

The first step in creating a "Lab on a Chip" device is to design the experimental setup needed to trap and excite fluorescence of a fluorescent particle. The first specification in the design was that a separate trapping laser needed to be used to trap the particle due to the high powers needed from an excitation source. The fluorescent particles used require a wavelength of about 532 nm to excite fluorescence within the particle. Therefore, using an excitation laser as the excitation and trapping source seems to be an efficient way to simplify the setup. However, due to the high powers needed to trap a particle with a 532 nm trapping source, this is not the case. A few watts, ~5 mW, are needed to trap a 1 μm diameter dielectric particle using this laser source. This high power causes the fluorescence in the particle to photo bleach within a few seconds, and is powerful enough to photo bleach surrounding particles that are not being simultaneously trapped. Therefore a second trapping laser at a much lower power is needed to trap the particle. A trapping laser at 800 nm with only a power of ~10 mW is used to trap the particle. Figure 8.1.1 shows a picture of such a trapped particle. Because the wavelength is far from 532 nm, this laser does not excite fluorescence and has a low enough power not to adversely affect the particles.

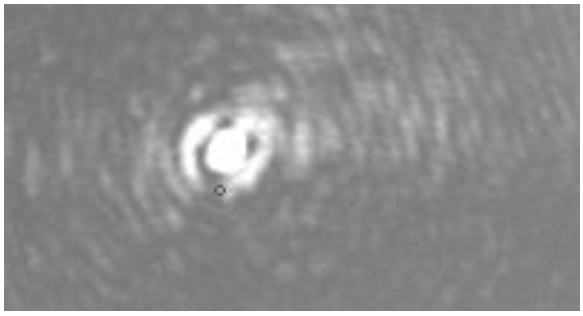

Figure 8.1.1: 2 µm diameter dielectric particle trapped using a 800 nm excitation source.

An inverted microscope is chosen in the design such that the backscattered light from the trapping and excitation lasers can be used to image and measure the fluorescence of the particle. Section 7.1 and figure 7.1 describe the experimental setup designed. Two separate beam paths for the trapping and excitation laser needed to be directed into the microscope such that they are incident on a sample to within a few nano or micro meters depending on the size of the particle. This is an extremely crucial step in the experimental setup. Failure to align the two beams to within this range causes the excitation laser to miss the trapped particle and produce fluorescence on an undesired particle.

The last major consideration in the experimental design was whether to use the wide field or the confocal setting of the inverted microscope. There are advantages and disadvantages to consider for each setting. For wide field, the major advantage is that by illuminating the entire sample the intensity of the laser is spread across the entire surface area of the sample. Therefore the florescence of many particles can be measured and photo bleaching is reduced due to the lower intensity. The advantage of using confocal is that the incident light is focused onto only one particle. This allows only one particle to be measured at a time in the location of the trapping laser. The disadvantage of wide field is that the fluorescence measured is not from a single particle. For confocal, the disadvantage is that the intensity of the

laser in the path is so powerful that the particle easily photo bleaches. Because the confocal setting allows only one sensor to be measured, this benefit outweighs all the disadvantages.

Because the confocal setting was used, the last feature of the design of the experimental setup was to add neutral density filters to the excitation laser path such that the power could be decreased to minimize photo bleaching. A neutral density wheel with a gradient of neutral densities could be used to find the ideal position to excite the particles with minimal photo bleaching. Using the highest setting, the excitation was reduced to a power between 10-100 μW. This allowed for enough power to excite fluorescence such that it could be measured with the USB 2000 software while also cutting down the photo bleaching to several minutes, which is enough time to allow for stable measurements.

8.1.2 Proof of Concept of Experimental Setup Using Commercial Fluorospheres

To demonstrate proof of concept of the experimental setup, commercial Fluorospheres with known fluorescence, see figure 7.2, were used. These commercial spheres were used instead of the nano-sensors because their fluorescence is well documented, while the nano-sensors are still in their fabrication stage. Figure 8.1.2 shows the fluorescence measured from a single Fluorosphere using the newly designed experimental setup. The particle was trapped with the 800 nm trapping laser at 10 mW, and excited with 532 nm at a power of 100 μW. The fluorescence is measured in arbitrary units versus wavelength of the fluorescent light.

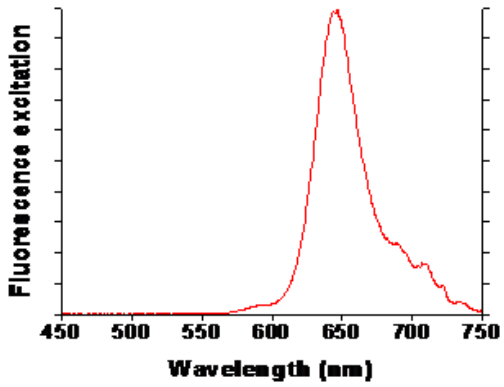

Figure 8.1.2: Fluorescence measurement of commercial 1 µm Fluorosphere using a 532 nm excitation laser and 800 nm trapping laser. The spectrum peaks at 650 nm and has the same behavior as the commercial spectra provided by the manufacturer of the spheres.

Comparing this fluorescence measurement with the commercial spectra shown in figure 7.2, it can be seen that the behavior of each measurement is very similar. Each spectrum has a peak emission at 650 nm, decaying quickly to 600 nm, and more slowly to 750 nm. Because the commercial particles are not ideal, the spectra from the experimental setup differs slightly from that of the commercial spectra. This may be due to slight misalignments of the beam paths, or due to imperfections in the dielectric material. Because the spectra of the Fluorospheres were able to be replicated with minimal error, this measurement verifies the proof of concept of the experimental setup. Therefore the next step is to begin characterization of the nano-sensors using this successful setup.

8.2 Characterization of Fluorescence Measurements of the Ion Selective Nano-sensors

Before the nano-sensors were introduced into the experimental setup, the first design for the fabrication of the nano-sensors was characterized. These spheres were trapped and

excited with only the 532 nm excitation source at a power of ~10 mW because the experimental setup design was also in its fabrication stage. Figure 8.2.1 is the fluorescence spectra of two different samples of nano-sensors at different pHs, one solution of pH ~2 and the other pH ~6, and sizes of 6 µm. The experiment was to show that the spectra measured from the two solutions should vary.

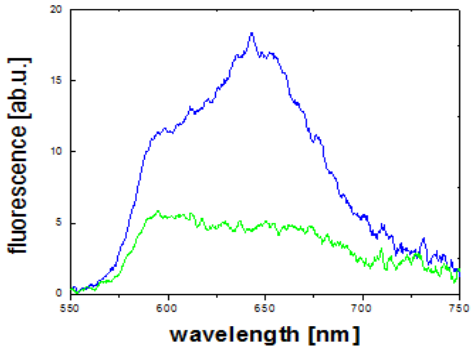

Figure 8.2.1: Fluorescence measurement of 6 µm pH sensitive nano-sensors using a 532 nm excitation laser and 800 nm trapping laser. The two solutions are distinguished by their solution color, blue (pH ~2) and green (pH ~6). The spectra of the blue solution peaks at 650 nm, and the green at 600 nm. Because the spectra differ this shows that the spectra can be used to distinguish between different pH solutions.

From figure 8.2.1 it can be seen that the spectra from the two solutions were indeed different. Both peaks should be the deprotonated peak as in figure 7.4, however the behavior is indistinguishable. The blue solution peaked at 650 nm, whereas the green peaked closer to 600 nm, however photo bleaching causes significant variance between the spectra, and therefore the behavior does not quite match the deprotonated behavior expected from figure 7.4.

Two issues with the spectra arose. The first was that, because the sensors were trapped with the excitation laser, photo bleaching was a significant problem. This can especially be seen in the green solution. The peak is not as intense as the blue solution, and this was significantly

caused by quick photo bleaching of the solution. This only verified the decision to trap with a separate laser when designing the final experimental setup. The second issue was that the fluorescence functionally is dependent on size. The smaller the particle, the more easily it can be damaged. The green spectra may have had smaller particles and therefore encountered significantly more photo damage. The peak placement and shape could not be verified in this experimental run. The only conclusion, although extremely important, was that changes in spectra of different pH solutions of the nano-particles could be detected by a difference in their fluorescence spectra.

Once the experimental setup was verified, see section 8.1.2, then the fluorescence of the nano-sensors were characterized. The solution was basic at a pH ~6. Based on the chemistry of the nano-sensors, see section 7.1, the peak of this solution should resemble that of a deprotonated one. Figure 8.2.2 shows preliminary data of a basic solution in the newly designed experimental setup.

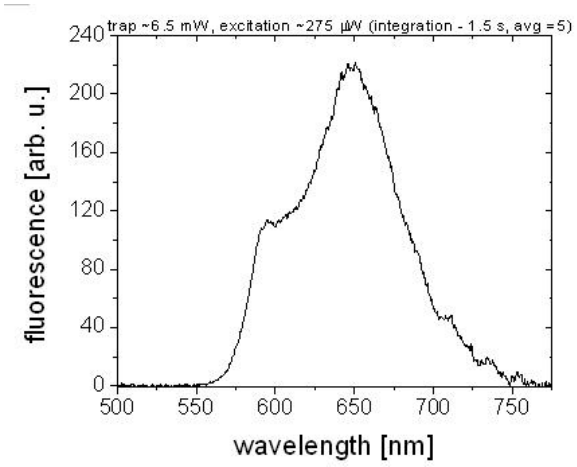

Figure 8.2.2: Fluorescence measurement of 6 µm pH sensitive nano-sensors using a 532 nm excitation laser and 800 nm trapping laser. The the solution is of blue (pH ~2) nano-sensors. Based on figure 7.4 the behavior of the sensor should resemble a deprotonated peak, and this data matches fairly well with this expected behavior.

This data confirms that the basic solution does behave as a deprotonated solution. The peak is also located at 650 nm, just as is in figure 7.4. Because the spectrum is deprotonated, and behaves as expected, then the characterization of the pH sensitive ions in the new experimental setup is verified.

The following data was taken by Mark Kendrick, a graduate collaborator on the "Lab on a Chip" project. Figure 8.2.3 shows fluorescence measurements of a K^+ ion sensitive nano-sensor at four second intervals. The data shows that as the K^+ gradient is introduced to the sensors, the deprotonated peak begins to dominate. This data was taken in wide field to reduce photo bleaching and imaged with a larger spectrometer slit. A new chromoionophore dye was used in the solution, therefore the peaks do not align exactly with figure 7.4, but the functionality of the solution is just the same.

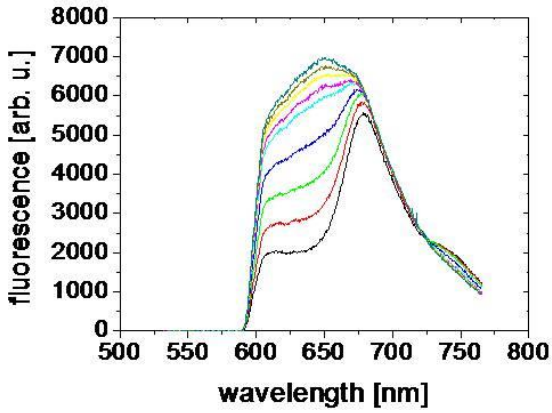

Figure 8.2.3: Fluorescence measurement of K^+ ion sensitive nano-sensors using a 532 nm excitation laser, 800 nm trapping laser, and a larger slit size spectrometer. Each spectra is taken at 4 second time intervals. As time elapses the deprotonated peak begins to dominate as the ion gradient increases.

This data only further verifies the functionality of the experimental setup. Because the nano-sensors behaved as predicted, and the deprotonated peak begins to dominate over time,

then the characterization of the sensors using the newly designed experimental setup is verified. The next step is to reproduce the same data but inside a microfluidic device.

8.3 Characterization of Fluorescence measurements inside a Microfluidic Device

One major goal of the "Lab on a Chip" project is to use the new experimental design to trap nano-sensors inside a microfluidic device. Figure 8.3.1 is a pictorial representation of trapping the nano-sensor in a simple microfluidic device. The microscope slide sample is to be replaced by the microfluidic device, but no other component of the experimental setup should need to be changed to conduct these experiments.

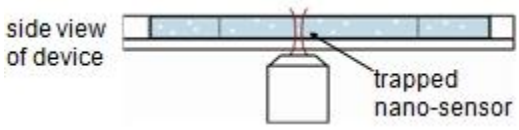

Figure 8.3.1: Pictorial representation of a trapped nano-sensor in a microfluidic device using the newly developed experimental setup.

The following data was again taken by Mark Kendrick. Figure 8.3.2 shows the fluorescence peak from two different pH solutions with nano-sensors. The first solution, with a pH of 2, peaks at 670 nm, and the second solution, at a pH of 8.5, peaks at 695 nm. This verifies that the acidic solution peaks at a higher wavelength than that of the basic solution. Again, a new chromoionophore dye was used in the solution, therefore the peaks do not align exactly with figure 7.4, but the functionality of the solution is just the same.

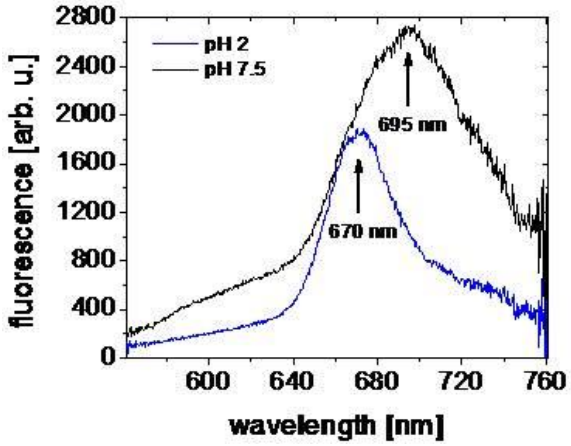

Figure 8.3.2: Fluorescence measurement of pH sensitive nano-sensors using a 532 nm excitation laser and 800 nm trapping laser inside a microfluidic device. The peak of the pH 2 sensor is at 670 nm, and the peak of the pH 8.5 solution is at 695 nm. This verifies that the acidic solution peaks at a higher wavelength then the basic solution.

This data demonstrates that the functionality of the experimental design allows the nano-sensors to be trapped inside a microfluidic device. Because the peaks of the pH solutions behave as expected, this means that there are no issues in contention with the experimental setup and microfluidic devices. It was unknown whether the setup would be compatible with the microfluidic devices, however with this successful data, it can be seen that the experimental setup is successful. Not only has the experimental setup been verified, but the characterizations of the nano-sensors can also be conducted in the setup with and without the microfluidic device.

9. Conclusions

The purpose of this project was to design the experimental setup needed to trap and excite fluorescence of a fluorescent particle or nano-sensor. For the project an excitation laser at 532 nm was needed as well as a optical trapping laser at 800 nm. It was discovered that the power of the excitation laser needed to be ~10 mW, which is low enough to cause minimal photo bleaching of the particles. The power of the trapping laser was found to be ~5 mW for a 1 µm particle. The crucial step in developing this design was to align both lasers to hit the sample on the inverted microscope to within a few nano-meters to ensure that the same particle trapped is the one excited. The other feature of the design was to use confocal imaging which focuses all the light onto only one particle. The advantage is that only one particle is being measured at a time, but the disadvantage is that this causes higher power which corresponds to more photo bleaching.

Proof of concept of the setup was then conducted using commercial Fluorospheres. The spectra measured by this design matched the theoretical spectra provided by the particles manufacturer, which verifies the setup. Next, measurements were taken on the nano-sensors made by the chemistry department. First using only the excitation laser to excite and trap the sensors, different fluorescence peaks were measured for two particle solutions of pH ~2 and pH ~6. The only uncertainty was in whether the peaks' behavior were that of deprotonated peaks as is expected. Because of photo bleaching this behavior was indistinguishable, however there was notable difference between the particles which was good. Next, the trapping laser was reintroduced and figure 8.2.2 verifies that fluorescence measurements of a nano-sensor can be obtained with this experimental design.

Two other experiments conducted by Mark Kendrick were done, which confirmed the proof of concept of this experimental design. Figure 8.2.3 has data of K^+ ion sensitive sensors which switch from deprotonated dominant peaks, to protonated, using widefield. This showed that the sensors behave as expected, and that the experimental design provided the materials needed to demonstrate this. Finally the experimental technique developed by Mark was able to trap and measure the fluorescence of pH 2 and pH 7.5 sensors inside a microfluidic device, and showed that the correct measurements can be taken with the set up.

Future experiments need to be conducted to characterize the sensors using this setup. Because the sensors are in their experimental design as well, inconsistencies in their fabrication have yielded inconsistent fluorescence measurements in this system. Therefore more testing of these particles is needed. The major error in the experimental design itself is the high powers due to confocal imaging that photo bleach the particles within minutes. Confocal imaging has the advantage that only one particle at a time is measured, however further experiments using widefield excitation conducted by Mark Kendrick, seem to indicate that photo bleaching is significantly reduced, and therefore widefield excitation may be more advantageous to use.

Future experiments are also being designed so as to use a new spectrometer that can image and measure spectra from multiple particles at a time. This will allow for time dependent measurements of the sensors to be conducted within the microfluidic. Therefore, using this new spectrometer, effects of the gradient at various positions and particles can all be measured with time. The final goal of this project is to introduce cells into the system and monitor the changes due to ion gradients using the experimental setup and sensors. The hope is to have a prototype of a “Lab on a Chip” system that can make the sensors *in situ* in the device and then directly measure changes within a cell.

10. Acknowledgments

I would like to thank Oksana Ostroverkhova for advising me on this project and helping me with my thesis and research both intellectually and emotionally. Special thanks goes to Mark Kendrick, my graduate student advisor, for helping me take most of this data, teaching me how to do this research, and for providing extra data that contributed to the proof of concept of the experimental design. I would also like to thank the entire Photonics and Electronics Laboratory at OSU for helping me with my research and making this a fun community to do research within. I would also like to thank David McIntyre for being my secondary advisor and the rest of the ONAMI team at OSU which includes the collaborators in the chemistry department.

I would also like to thank the 2011 senior class in physics at OSU for revising and helping me do edits on my thesis. A big thanks also goes out to my senior thesis teacher Janet Tate for helping us plan out and efficiently going about the thesis, and for being generous to make corrections to the thesis which only improved its quality. Finally, a special thanks goes out to my boyfriend, Daniel Gruss, who helped me work through some design and computational aspects of my project. He worked in a optical trapping group as well so his intellectual help and collaborative research was a definite advantage in doing this thesis project.

I would also like to thank the National Science Foundation, the Oregon Nanoscience and Microtechnologies Institue, and the Office of Naval Research for funding this “Lab on a Chip” project.

Bibliography

[9] E. Eriksso, J Scrimgeour , et al., “Optical Manipulation and Microfludics for Studies of Single Cell Dynamics,” Journal of Optics A: Pure and Applied Optics **9** S113-21 (2007).

[10] D. McIntyre, “Injected K^+ ion Nanosensors into Cells,” Unpublished picture, Dept. of Physics, Oregon State University (Corvallis, OR), 2010. <http://www.physics.oregonstate.edu/~mcintyre/optodes.html>.

[11] A. Ashkin, “Life Fellow 200 History of Optical Trapping and Manipulation of Small-Neutral Particle, Atom, and Molecules,” IEEE Journal on Selected Topics in Quantum Electronics. **6** 841-55.

[12] V. Bychkova and A. Shvarev, "Fabrication of Micrometer and Submicrometer-Sized Ion-Selective Optodes via a Solvent Displacement Process," Anal. Chem. **81**, 2325 (2009).

[13] M.T. Koesdjojo, et. al., “Two-stage polymer embosing of co-planar microfluidic features for microflidic devices,” Sensors and Actuators B **131**, 692 (2008).

[14] N. Finetti, et. Al., “Study of Test-mass Charging Process in the LISA Mission Due to Diffuse γ-rays,” Journal of Physics: Conference Series **154** (2009).